Available online at www.sciencedirect.com
ScienceDirect
Surface & Coatings Technology 202 (2007) 768 – 773
SURFACE & COATINGS TECHNOLOGY
www.elsevier.com/locate/surfcoat

Microstructure evolution and dielectric properties of $Ba_{0.7}Sr_{0.3}TiO_3$ parallel plate capacitor with Cr interlayer

Chia-Cheng Ho [a], Bi-Shiou Chiou [a,b,*], Li-Chun Chang [c]

[a] Institute of Electronics, National Chiao-Tung University, Hsinchu, Taiwan
[b] Innovative Packaging Research Center, National Chiao-Tung University, Hsinchu, Taiwan
[c] Department of Electronic Engineering, Huafan University, Taipei, Taiwan

Available online 24 May 2007

Abstract

The microstructure, crystalline phase, surface morphology, and dielectric properties of a sandwich structure of $Ba_{0.7}Sr_{0.3}TiO_3$/Cr/$Ba_{0.7}Sr_{0.3}TiO_3$ (BST/Cr/BST) dielectric are characterized to understand the influence of the nano-Cr interlayer. BST dielectrics inserted with Cr film of thickness ranged from 2 nm to 15 nm all show the crystalline cubic phase. However, TiO_2 layer is formed on the upper BST layer after the BST/Cr/BST dielectrics are annealed at 800 °C in O_2 atmosphere for one hour. In this study, TEM, AFM, SEM, X-ray diffraction, and AES are employed to investigate the microstructure evolution of the BST/Cr/BST dielectrics after annealing. The correlations between the microstructure and the dielectric properties of the Pt/BST/Cr/BST/Pt capacitors with various Cr thicknesses are explored.
© 2007 Elsevier B.V. All rights reserved.

Keywords: Dielectric material; Interlayer; Microstructure; Capacitor; BST

1. Introduction

Recently, there has been a great interest in the development of thin film ferroelectric materials because of their growing use in piezoelectric, optical, and electrical devices. $Ba_xSr_{1-x}TiO_3$ (BST) has been considered as a suitable dielectric material for integrated, nonvolatile memories, dynamic random access memories (DRAMs), bypass capacitors, and IR capacitors. BST films also show the low leakage current, high breakdown field, high time-dependent dielectric breakdown (TDDB), and low fatigue and aging [1–3]. However, the operating temperatures may range from room temperature to about 125 °C, and the dielectric constant of BST films varies with the operating temperature [4–6].

Dielectric behaviors of BST thin films can be modified with an underlayer [7–9] and various dopants [10–13]. On the other hand, stack insulator structure of dielectrics shows excellent dielectric properties [14], and nanocomposite capacitor shows the promising dielectric properties with the ceramic fillers [15,16]. This is on-going research. Inserted Cr into BST films can decrease the temperature dependence of capacitance [5]. Annealing in different atmospheres [4] can change the microstructure of BST/Cr/BST sandwich structure. Our previous study suggests the formation of TiO_2 films after 800 °C annealing in O_2 atmosphere for

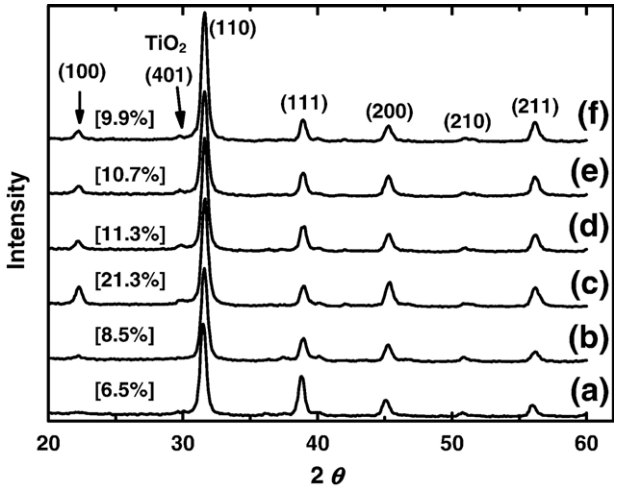

Fig. 1. X-ray diffraction patterns of BST/Cr/BST with a Cr thickness of (a) 0 nm (as-deposited specimen); (b) 0 nm; (c) 2 nm; (d) 5 nm; (e) 10 nm; and (f) 15 nm. Samples (b)–(e) are annealed at 800 °C in O_2 atmosphere for one hour. Datum in the brackets is the ratio of I(100) to I(110) of BST films.

* Corresponding author. Institute of Electronics, National Chiao-Tung University, Hsinchu, Taiwan. Tel.: +886 3 5731927; fax: +886 3 5731590.
E-mail address: bschiou@mail.nctu.edu.tw (B.-S. Chiou).

0257-8972/$ - see front matter © 2007 Elsevier B.V. All rights reserved.
doi:10.1016/j.surfcoat.2007.05.077

one hour affects the dielectric properties of the BST/Cr/BST sandwich structures [5]. In this study, microstructure evolution of BST/Cr/BST sandwich structure is explored, and the effects of Cr thickness on the dielectric properties of MIM capacitors are investigated and correlated with the formation of TiO_2 layer.

2. Experimental procedures

Specimens of $Pt/Ba_{0.7}Sr_{0.3}TiO_3/Cr/Ba_{0.7}Sr_{0.3}TiO_3/Pt$ structure were employed. The starting p-type Si (100) wafers were cleaned by the standard RCA cleaning process. After cleaning, a 100-nm SiO_2 films were grown on the Si substrate by the dry-oxidation in 1000 °C for 30 min. A 10-nm Ti films were sputtered onto the SiO_2 layer in the DC sputtering system, while a DC voltage is applied across the two electrodes to create a plasma. The bottom electrodes, 100-nm thick Pt films, were dc sputtered at room temperature. The first $Ba_{0.7}Sr_{0.3}TiO_3$ (BST) films were then deposited using an RF magnetron sputtering at a substrate temperature of 350 °C for two hours, while RF voltages can be coupled capacitively through the insulating target to create a plasma. The sputtering chamber was evacuated to a base pressure of 1×10^{-5} torr. Then, BST films were deposited at a constant pressure of 5×10^{-3} torr which was maintained by a mixture of argon and oxygen at 9 sccm and 3 sccm, respectively. The RF power for the deposition of both the first and second BST layers was 120 W (power density was 2.7 W/cm^2) for two hours, and the total thickness of BST films was about 300 nm (deposition rate: ~1.25 nm/min). Chromium films with various thicknesses (2 nm, 5 nm, 10 nm, and 15 nm) were deposited after the deposition of the first BST films with

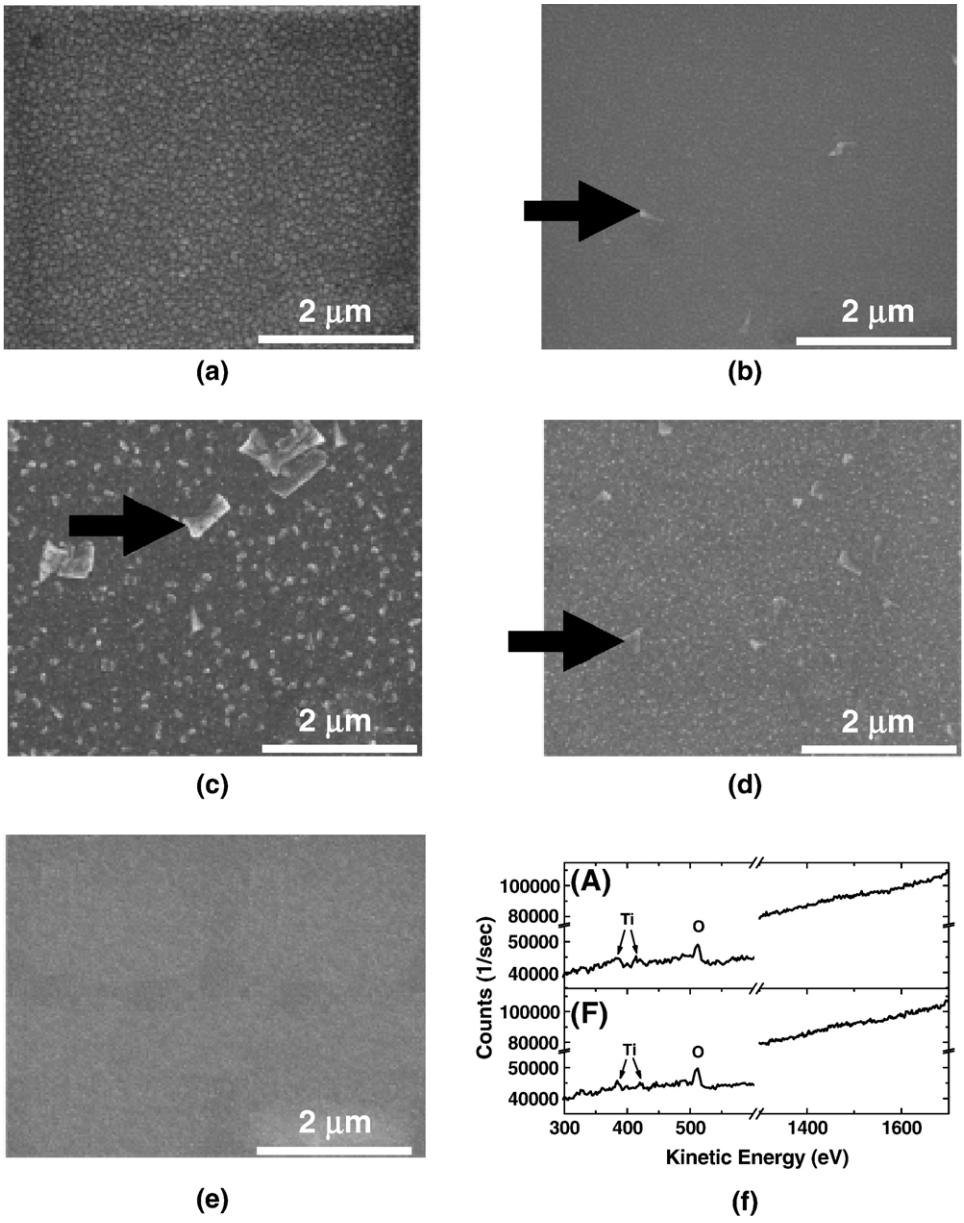

Fig. 2. Microstructure of BST/Cr/BST with a Cr thickness. (a) 0 nm; (b) 2 nm; (c) 5 nm; (d) 10 nm; and (e) 15 nm as the function of inserted Cr thickness after annealing at 800 °C in O_2 atmosphere for one hour. Aggregates are indicated by arrows. (f) Auger spectra of the aggregates (A) and the film surface (F).

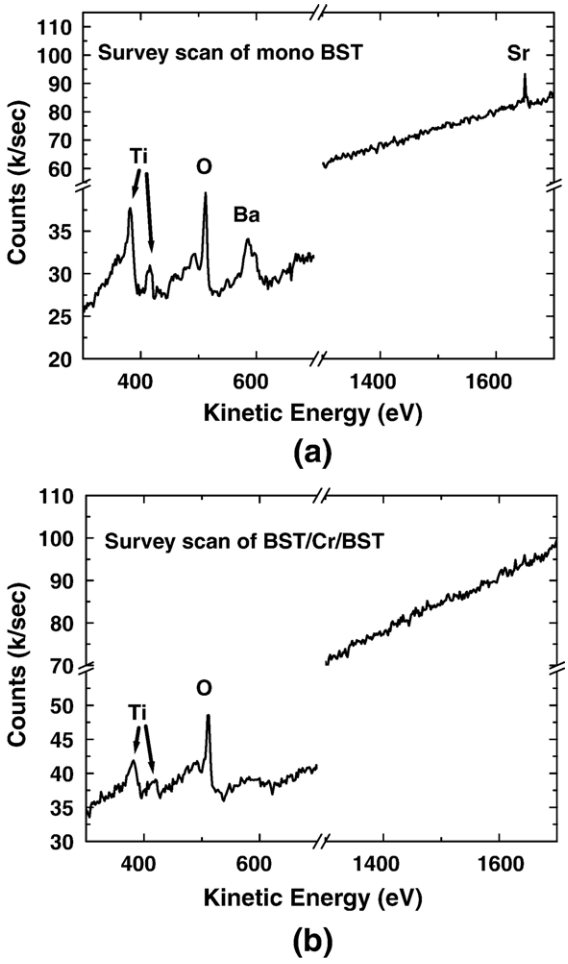

Fig. 3. Auger spectra of (a) BST and (b) BST/Cr(15 nm)/BST specimens.

the same sputtering system at a DC power of 100 W. The thickness of Cr films was monitored with a quartz crystal and a controller. The second BST layers were then deposited. The BST/Cr/BST/Pt specimens were annealed at 800 °C in O_2 atmosphere for one hour and then were bombarded by O_2 plasma for 10 min before deposition of the top Pt electrode.

A dual beam (focused ion beam and electron beam) system (Nova 200, FEI company, Japan) was employed to observe the surface morphology of the films. An atomic force microscope (AFM) (Digital instrument NS3a controller with D3100 stage, Veeco Instruments Inc., U.S.A.) was employed to study the surface morphology and roughness. The phase of the films was characterized by an X-ray diffractometer (XRD) (RU-H3R, Rigaku Co., Japan) at 0.154056 nm of the wavelength (λ). The film composition was investigated with Auger electron spectroscopy (AES) (Microlab 350, Thermal VG Scientific Co., England). The high resolution transmission microscopy (HRTEM) (JEM-3000F, JEOL Ltd., Japan) was employed to observe the cross-section of multilayer specimens, and a selected area electron diffraction (SAED) pattern was used to define the structure of the BST films. An LCR meter (HP-4285, Hewlett Packard Co., U.S.A.) was employed to study the dielectric constant and dissipation factor of the capacitors.

3. Results and discussion

The X-ray diffraction patterns of the BST films with Cr of various thicknesses are given in Fig. 1. All BST films show crystallized cubic phase. However, a diffraction peak appears at $2\theta = 29.70°$, and this peak is attributed to the formation of β-TiO_2 after the BST/Cr/BST dielectric are annealed at 800 °C in O_2 atmosphere for one hour. Datum in the brackets in Fig. 1 is the peak intensity ratio of I(100) to I(110) of BST films. Without the insertion of Cr interlayer, a preferred (110) orientation is found in the BST film as shown in Fig. 1(a). By inserting a 2-nm Cr interlayer, the ratio I(100)/I(110) of the BST films increases from 6.5% to 21.3% dramatically. The presence of (100) peak implies specific oriented grains, which enhances the dielectric constant of the BST because the Ti ion preferentially displaced along the (100) direction towards the oxygen ions [17].

Specimens with mono BST layer annealed at 800 °C in O_2 atmosphere for one hour exhibit the uniform microstructure with an average grain size of about 100 nm, as shown in Fig. 2(a). Heterogeneous microstructures with the aggregates as indicated by arrows shown in Fig. 2(b)–(d) are observed for BST/Cr/BST with Cr thicknesses ranging from 2 nm to 10 nm. Nevertheless, the microstructure of BST/Cr(15 nm)/BST exhibits a

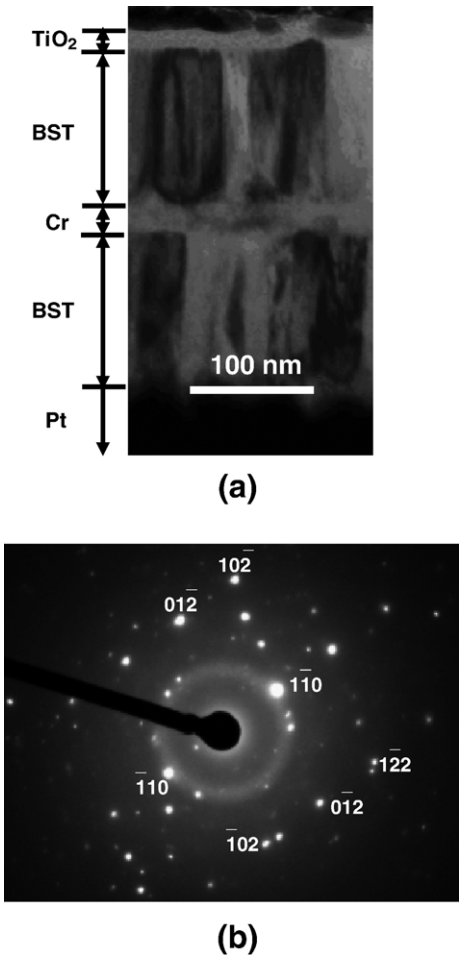

Fig. 4. (a) Cross-section photograph of BST/Cr(15 nm)/BST and (b) The SAED pattern of BST confirms the cubic perovskite BST phase.

homogeneous surface morphology as shown in Fig. 2(e). Auger analysis results, shown in Fig. 2(f), suggest that only Ti and O are present in both the aggregates (A) and the film surfaces (F).

Fig. 3(a) and (b) present AES survey scan profiles for BST films without and with 15 nm Cr, respectively. There are four elements (Ba, Sr, Ti, and O) on the surface of the BST film without Cr interlayer (Fig. 3(a)), however, only Ti and O elements appear on the surface of BST/Cr(15 nm)/BST specimen (Fig. 3(b)). On the basis of the XRD and the AES results, it is argued that TiO_2 layer is formed after the BST/Cr/BST films are annealed at 800 °C in O_2 atmosphere for one hour. Fig. 4(a) is the cross-section view of the BST/Cr(15 nm)/BST sample where there is a layer, presumably TiO_2, on top of BST. However, formed TiO_2 layer is thin, so the selected area electron diffraction (SAED) patterns reveal only the cubic perovskite BST phase. The SAED spots, instead of rings, are observed in Fig. 4(b) because the electron-beam was focused on

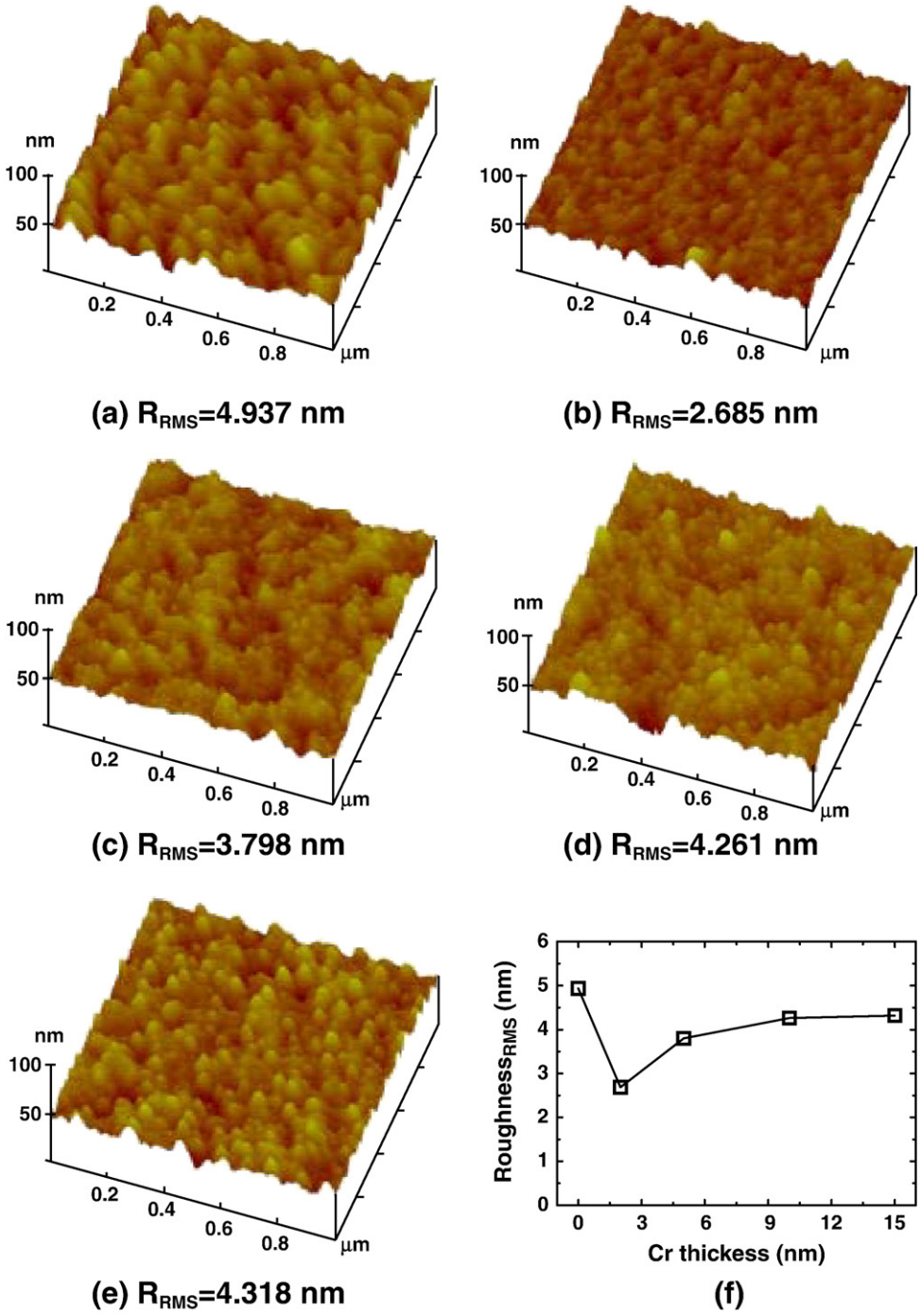

Fig. 5. Microstructure and root-mean-square (RMS) surface roughness (R_{RMS}) of BST/Cr/BST with a Cr thickness. (a) 0 nm; (b) 2 nm; (c) 5 nm; (d) 10 nm; (e) 15 nm; and (f) surface roughness as the function of inserted Cr thickness. Samples are annealed at 800 °C in $^{O}_{2}$ atmosphere for one hour.

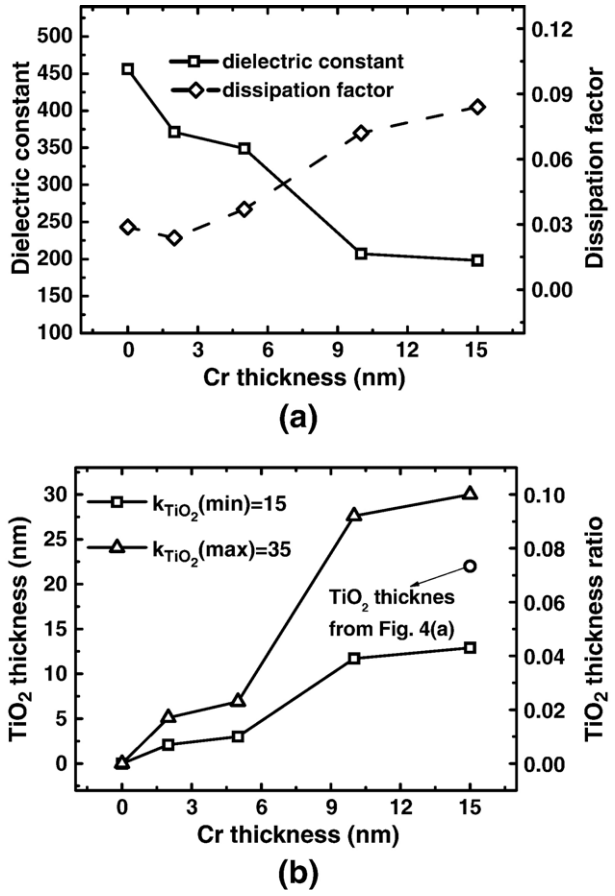

Fig. 6. (a) The 100 kHz dielectric constant and dissipation factor and (b) the calculated TiO_2thickness ($tTiO_2$) of BST/Cr/BST dielectric as a function of Cr thickness.

the BST grain. However, the formation of TiO_2 is not clear now, and further studies are in progress. The created new compounds of BST films are possible. According to our XPS data, the shift of Ti binding energy is not obvious. On the other hand, Cr^{+3} (0.130 nm) is difficult to replace Ti^{+4} (0.145 nm) in the pervoskite structure.

Fig. 5 give the AFM surface morphology and root-mean-square (RMS) surface roughness of specimens with various Cr thicknesses. The RMS surface roughness of mono BST film is 4.937 nm and the inserted Cr layer decreases the surface roughness, as shown in Fig. 5(f). The RMS values are 2.685 nm (t_{Cr}=2 nm), 3.798 nm (t_{Cr}=5 nm), 4.261 nm (t_{Cr}=10 nm), and 4.318 nm (t_{Cr}=15 nm). As indicated in Fig. 5(f), the RMS surface roughness decreases and then increases as t_{Cr} increases. It is argued that the rough surface is attributed to the presence of the aggregators as shown in Fig. 2.

Fig. 6(a) gives the dielectric constant (k) and dissipation factor (DF) of specimens with and without Cr interlayer at 100 kHz. The dielectric constant decreases as t_{Cr} increases. Comparing with mono BST capacitor (DF ~0.028), the dissipation factor (DF) decreases to 0.023 for specimens with 2-nm Cr layer, although the dielectric constant decreases from 456 to 371 with the implementation of 2-nm Cr interlayer. A preferred (100) orientation of BST suggests higher dielectric constant, and films with Cr show preferred (100) orientation as discussed previously. The dielectric constants of BST/Cr/BST dielectric are smaller than that of BST. Formation of TiO_2 is the root cause for the decrease of k. The TiO_2 dielectric is in serial with the BST dielectric. The dielectric constants of TiO_2 and BST are about 15–35 [18] and 456, respectively. The TiO_2 thickness (t_{TiO2}) calculated with the following equation based on serial capacitor model.

$$t_{TiO_2} = \frac{k_{TiO_2}}{C}A - \frac{k_{TiO_2}}{k_{BST}}t_{BST} \quad (1)$$

where C is the measured capacitance, A is the electrode area, $k^{TiO}{}_2$ ($t^{TiO}{}_2$) and k^{BST} (t^{BST}) are the dielectric constant (thickness) of TiO_2 and BST, respectively.

Fig. 6(b) gives the calculated TiO_2 thickness as a function of t_{Cr} with k_{TiO2}=15 and 35. The calculated t_{TiO2} ranges from 13 to 30 nm for BST/Cr(15 nm)/BST, which is consistent with HRTEM image in Fig. 4(a) where the TiO_2 thickness is estimated to about 22 nm.

4. Conclusions

In this study, parallel plate capacitors with BST/Cr/BST multilayer dielectric are investigated. The insertion of the 2 nm Cr reduces the surface roughness and dissipation factor of the dielectrics. SEM and AFM are employed to investigate the microstructure of the BST/Cr/BST dielectrics, and the heterogeneous microstructures with the aggregates are found. The TiO_2 layers are formed on the upper BST layer as suggested by X-ray diffraction patterns, TEM cross-section photograph, and AES analyses.

The dielectric constant (k) decreases as a function of the thickness of nano-Cr interlayer. A dissipation factor of 0.023 at 100 kHz is obtained for BST/Cr(2 nm)/BST MIM capacitor as compared to that of 0.028 for mono BST MIM capacitor. The decrease in k is attributed to the formation of TiO_2 films on the upper BST layer after the 800 °C annealing in O_2 atmosphere for one hour.

Acknowledgement

This work is sponsored by National Science Council, Taiwan, under the contract number NSC 95-2221-E-009-085.

References

[1] D.C. Shye, B.S. Chiou, M.J. Lai, C.C. Hwang, C.C. Jaing, J.S. Chen, M.H. Cheng, H.C. Cheng, J. Electrochem. Soc. 150 (2003) F20.
[2] D.C. Shye, B.S. Chiou, M.W. Kuo, J.S. Chen, B.C.S. Chou, C.C. Jaing, M.F. Wu, H.C. Cheng, Electrochem. Solid-State Lett. 6 (2003) G55.
[3] J.W. Liou, B.S. Chiou, J. Mater. Sci., Mater. Electron. 11 (2000) 637.
[4] C.C. Ho, B.S. Chiou, L.C. Chang, C.C. Chou, B.H. Liou, C.C. Yu, Surf. Coat. Technol. 201 (2006) 4163.
[5] C.C. Ho, B.S. Chiou, L.C. Chang, Appl. Phys. Lett. 90 (2007) 132906.
[6] M.W. Kuo, D.C. Shye, B.S. Chiou, J.S. Chen, H.C. Cheng, Integr. Ferroelectr. 61 (2004) 183.
[7] W.C. Yi, T.S. Kalkur, E. Philofsky, L. Kammerdiner, Thin Solid Films 402 (2002) 307.

[8] K.H. Yoon, J.H. Sohn, B.D. Lee, D.H. Kang, Appl. Phys. Lett. 81 (2002) 5012.
[9] J. Sigman, P.G. Clem, C.D. Norduist, Appl. Phys. Lett. 89 (2006) 132909.
[10] M.C. Chiu, Y.C. Lee, F.S. Shieu, J. Electrochem. Soc. 152 (2005) F194.
[11] S.Y. Chen, H.W. Wang, L.C. Huang, Jpn. J. Appl. Phys. 40 (2001) 4974.
[12] K.T. Kim, C.I. Kim, Thin Solid Films 472 (2005) 26.
[13] K.H. Yoon, J.C. Lee, J. Park, D.H. Kang, C.M. Song, Y.G. Seo, Jpn. J. Appl. Phys. 40 (2001) 5497.
[14] S.J. Kim, B.J. Cho, M.F. Li, S.J. Ding, C. Zhu, M.B. Yu, B. Narayanan, A. Chin, D.K. Kwong, IEEE Electron Device Lett. 25 (2004) 538.
[15] J.J. Si, H. Ono, K. Uchida, S. Nozaki, H. Morisaki, N. Itoh, Appl. Phys. Lett. 79 (2001) 3140.
[16] B.W. Lee, I.R. Abothu, P.M. Raj, C.K. Yoon, R.R. Tummala, Scr. Mater. 54 (2006) 1231.
[17] Y. Xia, D. Wu, Z. Liu, J. Phys. D: Appl. Phys. 37 (2004) 2256.
[18] R. Singh, S. Alamgir, R. Sharangpani, Appl. Phys. Lett. 67 (1995) 3939.